https://dx.doi.org/10.1016/j.tws.2016.10.013

Behaviour of concrete-filled cold-formed elliptical hollow sections with varying aspect ratios

Faqi Liu [a,b], Yuyin Wang [a,b], Tak-ming Chan [c]

[a]Key Lab of Structures Dynamic Behavior and Control (Harbin Institute of Technology), Ministry of Education, Heilongjiang, Harbin, 150090, China

[b]School of Civil Engineering, Harbin Institute of Technology, Heilongjiang, Harbin, 150090, China

[c]Department of Civil and Environmental Engineering, The Hong Kong Polytechnic University, Hong Kong, China

Abstract:

This paper presents the experimental and numerical studies of concrete-filled cold-formed elliptical hollow sections with varying aspect ratios subjected to axial compression load. Twenty one stub columns were tested to investigate the fundamental behaviours of these elliptical concrete-filled steel tubular (CFST) columns. The axial load versus displacement curves, longitudinal and transverse strains in steel tube and failure modes were obtained and discussed. A constitutive model for concrete in the elliptical CFST columns was proposed. Finite element (FE) models were developed and validated against the test results. Parametric studies were carried out to identify the influence of key parameters on the load-bearing capacity. Key parameters included aspect ratio, steel tube to concrete area ratio, yield strength of steel and compressive strength of concrete. Finally, the applicability of relevant design methods to elliptical CFST columns was assessed on the basis of the test and the FE results of this research and other related studies. Results indicated that the design method recommended in the Chinese Standard (GB50936-2014), and the design method for circular CFST columns in EC4 were found to generate accurate predictions.

Key words: concrete-filled steel tubular (CFST) column; elliptical section; confinement effect; stress -strain relationship

Nomenclature

a	major axis outer radius
b	minor axis outer radius
A_c	cross-sectional area of concrete core
A_s	cross-sectional area of steel tube
D_e	equivalent diameter
E_c	Young's modulus of concrete
E_s	Young's modulus of steel
f_{ck}	characteristic concrete strength, $f_{ck}=0.67\ f_{cu}$
f_{cu}	concrete cube strength
$f_{cu,28}$	concrete cube strength at 28 days
$f_{cu,test}$	concrete cube strength at the test day of specimens
f_c'	concrete cylinder strength
f_y	yield strength of steel
f_u	ultimate tensile strength of steel
H	height of column
N_y	yield load of composite column
N_u	cross-sectional capacity of composite column
t_s	wall thickness of the steel tube
α_s	steel tube to concrete area ratio, $\alpha_s=A_s/A_c$
ε	strain
ε_f	percentage elongation at fracture of steel
μ_Δ	ductility index
v_s	Poisson's ratio of structural steel
σ	stress
Δ_y	displacement at yield load
Δ_u	displacement at ultimate load
$\Delta_{0.85}$	displacement at $0.85N_u$ after peak load

1. Introduction

Elliptical hollow section has gained much attention, recently, from engineers due to its aesthetical appearance and structural efficiency [1]. Concrete-filled elliptical hollow sections further enhance the load-bearing capacity, ductility and seismic performance [2]. These enhancements are attributed to the composite action of steel tube and concrete, of which the steel tube provides confinement to the concrete, and in turn the concrete delays or prevents the local buckling of steel tube. The degree of the confinement offered by an elliptical cross-section to the concrete infill lies between that offered by a circular cross-section (with uniform confinement) and that offered by a rectangular hollow sections (with limited confinement) which further depends on the aspect ratio of the elliptical cross-section.

To date, extensive investigations have been conducted on the behaviours of the elliptical CFST columns. Yang et al. [2], Zhao and Packer [3], Uenaka [4] and Chan et al. [5] tested the axially loaded elliptical CFST stub columns. Sheehan et al. [6] investigated the eccentrically loaded elliptical CFST stub columns experimentally and numerically. Jamaluddin et al. [7] tested the axially loaded elliptical CFST stub and slender columns. Dai et al. [8, 9] numerically studied the axially loaded elliptical CFST stub columns and slender columns. Espinos et al. [10] conducted experiments on ambient and fire behaviours of eccentrically loaded elliptical CFST columns, filled with plain and reinforced concrete. Ren et al. [11] tested elliptical CFST beams and eccentrically loaded elliptical CFST slender columns. McCann et al. [12] carried out experiments on axially and eccentrically loaded elliptical CFST slender columns, filled with plain and reinforced concrete.

However, most of the above studies used hot-rolled elliptical hollow sections, and the steel tube to concrete area ratio was between 17% to 69%, which was higher than the common range of steel tube to concrete area ratio for CFST columns (4% to 20% [13]). Meanwhile, the aspect ratio (a/b) of all the commercially available hot-rolled elliptical hollow sections is 2.0, and the available dimensions of the hot-rolled section are limited, which may hinder a wider use of elliptical CFST columns in practice. Therefore, cold-formed elliptical hollow sections can be used to provide a wider range of sections for construction use. In this paper, the fundamental behaviour of cold-formed elliptical CFST columns with an aspect ratio ranging from 1.0 to 2.5 is investigated.

A series of tests was conducted to study the influence of aspect ratio and steel tube to concrete area

ratio on the behaviour of elliptical CFST stub columns. After that, a finite element (FE) model was developed, using the program ABAQUS, to simulate the behaviour of the elliptical CFST columns. A uniaxial compressive stress-strain relationship for concrete was proposed, which can account for the changes of the confinement effect of steel tube to concrete caused by the change in aspect ratio. Parametric studies were performed to identify the influence of key parameters on the load-bearing capacity of elliptical CFST columns. Finally, the test and FE results in this research, together with the test results of related studies, were compared with predictions of current codes and related design methods. The design method for elliptical CFST columns in Chinese code GB50936-2014 and the method for circular CFST columns in EC4 were found to yield good predictions for the concrete-filled cold-formed elliptical hollow sections.

2. Experimental program

2.1 General

Experiments were conducted to investigate the fundamental behaviours of the axially loaded elliptical CFST stub columns. Tests on elliptical hollow sections were also performed for comparison.

A total of 21 specimens, including 3 axially loaded elliptical hollow sections and 18 axially loaded elliptical CFST columns were tested. The key parameters were: aspect ratio a/b (1.0 to 2.5) and steel tube to concrete area ratio α_s (5% to 12%). The columns were labelled by the above-mentioned parameters. Taking the specimen *C20-5-a* for example, *C* denotes column; *20* represents the aspect ratio of 2.0; *5* refers to the steel tube to concrete area ratio of 5% while the finial letter identifies the different column in a group with the same parameters. In addition, group *CH20* corresponds to the elliptical hollow tubes. Detailed parameters of the specimens are given in Table 1, where a is the major axis outer radius, b is the minor axis outer radius, t_s is the thickness of the steel tube, H is the height of the column, α_s is the steel tube to concrete area ratio defined as A_s/A_c. A typical cross-section of the elliptical CFST column is shown in Fig.1. The height of all specimens was taken as $4a$ to ensure short column behaviour.

The elliptical steel tubes were cold-formed from steel sheets and seam welded. A steel sheet, with a nominal thickness of 2.75 mm, was used in the test. The steel tube to concrete area ratio was kept

constant while aspect ratio varied from 1.0 to 2.5, whereas the cross-sectional area varied to fulfil the variation of steel tube to concrete area ratio. The properties of the parent steel sheets were determined by performing tensile coupon tests according to the Chinese Standard GB/T 228-2010 [14] and were summarised in Table 2, in which E_s is the elastic modulus, f_y is the yield strength, f_u is the ultimate tensile strength, v_s is the Poisson's ratio and ε_f is the percentage elongation at fracture of the steel. Fig.2 illustrates a typical measured stress versus strain relationship of the parent steel. The coupon specimens were extracted from the parent steel sheets prior to the fabrication of the elliptical hollow section. As anticipated, the corner regions of the cold-formed steel sections have higher strength than the flat regions, due to the plastic deformation of the fabrication. Chan et al. [5] found that the strength of the corner region is 4% higher than that of the flat region in the cold-formed elliptical hollow sections. Compared to the gross section, the area of the corner regions is relatively small and its enhancement effect would be further minimised by the concrete infilling in the CFST column. Therefore the effect of corner region on the behaviour of elliptical CFST column would be limited.

The C40 grade concrete was used to fill the steel tubes. In order to evaluate the compressive strength and the elastic modulus, 150 mm ×150 mm ×150 mm cubes and 150 mm ×150 mm ×300 mm prisms were fabricated and cured under the same conditions as the specimens. The concrete mixtures and tested strengths are presented in Table 3, in which $f_{cu,28}$ and $f_{cu,test}$ are the concrete cube strength tested at 28 days after casting and at the test day of specimens, respectively, and $E_{c,test}$ is the elastic modulus at the test day.

2.2 Test setup and procedure

All specimens were tested in a 5000 kN hydraulic compression machine. Linear variable displacement transducers (LVDTs) were mounted to measure the axial displacements, as shown in Fig.3(a). Pairs of strain gauges were placed on the steel tube along the perimeter at the mid-height of the columns, in order to monitor the differences of strains at different locations and then to analyse the changes of confinement effect along the perimeter. The layouts of strain gauges are shown in Fig.3(b). The load, the corresponding axial displacements and the longitudinal and transverse strains were monitored and recorded during the test.

2.3 Test results and discussions

The elliptical hollow sections and elliptical CFST columns subjected to concentric loading failed by local buckling and shear failure of the concrete infill, respectively, as shown in Fig.4. The specimens upon removal of steel tube are also presented in Fig.4. Both inward buckling and outward buckling were observed in the elliptical hollow sections, however, only outward local buckling was observed in the steel tube of elliptical CFST columns, since inward buckling deformation of the steel tube was prevented by the concrete core. During the tests, the local buckling in the steel tube of elliptical hollow sections became apparent at load around 70% of the ultimate load. However, the local buckling in the steel tube of the elliptical CFST columns occurred at about 90% ultimate load. The delay of the local buckling in the steel tube may be attributed to the in-filled concrete.

The load versus axial displacement curves of the test specimens are illustrated in Fig.5. As observed, the initial behaviour was almost linear elastic up to around 0.75 times the ultimate load, followed by a ductile behaviour to the ultimate load, after which, the load decreases gradually with the increasing axial displacement. Table 4 shows the yield load (N_y), the displacement at the yield load (Δ_y), the ultimate load (N_u), the displacement at the ultimate load (Δ_u), the displacement at $0.85N_u$ after peak load ($\Delta_{0.85}$), and the ductility index (μ_Δ), in which the yield load and the ductility index were determined by the methods described in [15].

For ease of comparison, the average stress ($\sigma_{aver}=N_u/(A_s+A_c)$) is also listed in Table 4. The stress in the steel tube of the elliptical hollow sections is less than the yield strength of steel since local buckling occurred prematurely. The average stress decreases to 2.1%, 5.6% and 16.0%, respectively, for elliptical CFST columns with an aspect ratio of 1.5, 2.0 and 2.5, relative to the circular specimen (a/b=1.0) (Fig.6(a)). And the ductility index decreases more significant than the average stress with an increase in aspect ratio, reaching 13.6%, 37.6% and 47.5%, respectively, for specimens with an aspect ratio of 1.5, 2.0 and 2.5, relative to the circular specimen (Fig.6(b)). This may be explained by the deterioration of confinement effect with an increase in aspect ratio.

The average stress and ductility index tend to increase with the increasing steel tube to concrete area ratio (Fig.7), though there are some discrepancies for the ductility index. Specifically, the average stress increases by 27.3% and 41.0%, respectively, for specimens with the steel tube to

concrete area ratio of 8% and 12%, relative to the specimen with a steel tube to concrete area ratio of 5%. This may be explained by the direct contribution of steel tube and the enhanced confinement effect caused by the increasing steel tube to concrete area ratio.

For the elliptical CFST column, the confinement of the steel tube to concrete varies along the perimeter due to the variation of the curvature. The longitudinal and transverse strains in the steel tube were measured during the test in order to analyse the stress state of the steel tube. Due to the symmetry of the layout of strain gauges, as shown in Fig.3, the typical locations can be summarised into two points and four points for the circular section and elliptical section, respectively (Fig.8). The transverse stresses in the steel tube are calculated from the measured longitudinal and transverse strains, using the elastic-plastic analysis method described in [16], and illustrated in Fig.9. For the circular section (a/b=1.0), the transverse stress at point A almost equals to that at point D, confirming the uniformity of confining force in the circular specimen. However, the transverse stress tends to increase from point A to point D for the elliptical sections (a/b=1.5 - 2.5). The changes of the transverse stress may be caused by the variation of the out-of-plane stiffness along the perimeter of the elliptical steel tube. Taking point D for example, its radius of curvature is larger and the corresponding out-of-plane stiffness is smaller than other points along the perimeter, therefore the corresponding transverse stress is larger than that of other points, and then the confining stress would be smaller than other points. In addition, the load corresponding to the onset of yield of steel tube grows closer to the ultimate load with the increasing aspect ratio. This may be attributed to the reduction of enhancement of load-bearing capacity with the increasing aspect ratio.

3. Finite element (FE) analysis

3.1 FE model

Finite element (FE) models were developed using the FE package ABAQUS to extend the range of the examined parameters in this study. Han et al. [17] proposed stress versus strain relationships of concrete in circular and square CFST columns, which were successfully adopted to simulate CFST stub columns and slender columns subjected to pure compression, bending, torsion and combined loading conditions. In this paper, a new stress versus strain relationship model was developed for the concrete in elliptical CFST columns, by introducing the effect of aspect ratio into the model

from Han et al. [17] as shown below:

$$y=\begin{cases}2x-x^2 & x\le 1\\ \dfrac{x}{\beta_0(x-1)^2+x} & x>1\end{cases} \tag{1}$$

in which $x=\varepsilon/\varepsilon_0$, $y=\sigma/\sigma_0$, $\xi=f_yA_s/f_{ck}A_c$, $\sigma_0=f_c^{'}$, $\varepsilon_0=\varepsilon_c^{'}+800\xi^{0.2}\times10^{-6}$, $\varepsilon_c^{'}=(1300+12.5f_c^{'})\cdot10^{-6}$, $\beta_0=(2.36\times10^{-5}\times(a/b)^5)^{[0.25+(\xi-0.5)^7]}\cdot(f_c^{'})^{0.5}\cdot0.5\ge0.12$, where f_y is the yield strength of the steel tube, A_s and A_c are the cross-sectional areas of the steel tube and the concrete, respectively, f_{ck} is the characteristic concrete strength and equals 0.67 times the concrete cube strength (f_{cu}), and $f_c^{'}$ is the concrete cylinder strength. The initial elastic modulus was taken as $4700\sqrt{f_c^{'}}$ N/mm^2, as recommended in the ACI specification [18].

The descending part of the stress versus strain curve becomes steeper as the aspect ratio increases (Fig.10), which reveals the corresponding deterioration of confinement effect. When the aspect ratio equals to 1.0, the new model coincides with the model proposed by Han et al. [17].

The concrete damaged plasticity model in ABAQUS was employed for the concrete including the description of the tensile behaviour of the concrete. A linear stress versus strain relationship, during both the ascending and descending phases, was defined for the tensile behaviour of concrete [15] and is given as follows:

$$\sigma=\begin{cases}E_c\varepsilon & \varepsilon\le\varepsilon_{cr}\\ f_t^{'}\left(\dfrac{\varepsilon-\varepsilon_{tu}}{\varepsilon_{cr}-\varepsilon_{tu}}\right) & \varepsilon_{cr}<\varepsilon\le\varepsilon_{tu}\\ 0 & \varepsilon>\varepsilon_{tu}\end{cases} \tag{2}$$

where

$$f_t^{'}=0.1f_c^{'},\quad \varepsilon_{cr}=\frac{f_t^{'}}{E_c},\quad \varepsilon_{tu}=15\varepsilon_{cr}$$

To define concrete damaged plasticity, the dilation angle, the flow potential eccentricity, the ratio of initial equibiaxial compressive yield stress to initial uniaxial compressive yield stress, the ratio of the second stress invariant on the tensile meridian and the viscosity parameter were defined to be 36°, 0.1, 1.16, 2/3 and 0, respectively, most of which is recommended for the normal strength concrete by the ABAQUS analysis user's manual. The classical metal plasticity model with Mises

yield surfaces and associated plastic flow, was used for the steel tube. The uniaxial behavior of the structural steel was defined by a five-stage elastic-plastic stress versus strain relationship [17].

The steel tube and concrete was modelled with 4-noded shell element S4R and 8-noded solid element C3D8R, respectively, as shown in Fig.11. The interactive behaviour between the steel tube and concrete was simulated using the interaction algorithm in ABAQUS. The inner surface of steel tube and outer surface of concrete were defined to be a contact pair, of which the former acts as slave surface and the latter acts as master surface. The property definition for the contact pair uses the Coulomb model of friction in the tangential direction, with a friction coefficient of 0.3, and "hard" contact model in the normal direction. For steel hollow sections, the initial geometrical imperfection was taken as the lowest buckling mode shape with an amplitude of $t_s/100$ [19, 20], where t_s is the wall thickness of the tube. Residual stresses were not measured and were not considered in the FE model. For CFST stub columns, the influence of local imperfection and residual stress are negligible due to the inner concrete [21], and therefore they were not incorporated into the FE model.

For the columns, the top and bottom ends of steel tube and concrete were fixed against all degrees of freedom except the axial displacement at the loaded end. A static stress analysis method was used and the displacement controlled analysis was performed to obtain the load versus displacement curves of these columns.

3.2 Verification of the FE model

The FE model was validated against the test results in this research. The comparisons between FE and test results are shown in Fig.12 and Table 5, which confirms that the FE model and the proposed stress versus strain relationship model can accurately predict the behaviour of the elliptical CFST columns.

The tests conducted by Yang et al. [2], Zhao and Packer [3], Uenaka [4], Chan et al. [5] and Jamaluddin et al. [7] were also employed to validate the FE model. The comparisons between FE and test load-bearing capacities of these tests, together with results in this study, are illustrated in Fig.13 and Table 6. The FE model underestimates the load-bearing capacity of the columns tested by Uenaka [4], which may be attributed to the end effect in the test, because the length of these

specimens was 1.0 to 1.5 times 2*a*. After excluding Uenaka's tests, the mean and standard deviation of the ratio of the FE-to-test load-bearing capacities are 1.048 and 0.086, respectively.

3.3 Parametric studies

Following the validation of the FE models, parametric studies were conducted to identify the influence of key parameters on the behaviour of the elliptical CFST stub columns. The considered parameters were aspect ratio (from 1.0 to 2.5), steel tube to concrete area ratio (from 4% to 20%), and strengths of steel (from 235 MPa to 420 MPa) and concrete (from 30 MPa to 60 MPa). The typical predicted load versus axial displacement curves and load bearing capacity are presented in Fig.14 and Fig.15, respectively. As observed, the aspect ratio has considerable influence on the load-bearing capacity and ductility, both of which decrease with the increasing aspect ratio, due to the reduction of confinement effect. The load-bearing capacity and ductility increase with the increasing steel tube to concrete area ratio and yield strength of steel, mainly due to the contribution of steel part, but also the enhancement of confining effect. The confinement effect of steel tube to the concrete decreases with the increasing of concrete strength, therefore the load-bearing capacity increases but the ductility decreases with the increasing concrete strength.

4. Design method

Among the current design codes for CFST columns, only the Chinese code GB50936-2014 [22] covers the elliptical CFST column. The method provided by the GB50936-2014 accounts for the influence of aspect ratio on the load-bearing capacity, however, it is mainly derived from numerical studies and requires further validation against experimental investigation. The cross-sectional capacity of the elliptical CFST column can be calculated as follows according to GB50936-2014:

$$N_{u,GB} = f_{sc}(A_s + A_c) \tag{3}$$

where

$$f_{sc} = (1.212 + B\xi + C\xi^2) f_c \tag{4}$$

$$B = (0.176 f_y / 213 + 0.974)(\frac{b}{a})^{0.3} \tag{5}$$

$$C = (-0.104 f_c / 14.4 + 0.031) \times (\frac{b}{a})^{0.3} \tag{6}$$

$$\xi = \frac{f_y A_s}{f_c A_c} \tag{7}$$

where f_{sc} is the compressive strength of the composite member, A_s and A_c are the cross-sectional area of steel tube and concrete, respectively; f_y and f_c are the yield strength of steel and compressive strength of concrete, respectively; a and b are the major axis outer radius and minor axis outer radius, respectively.

Yang et al. [2], Zhao and Packer [3] and Chan et al. [5] found that the design method for square and rectangular CFST columns in EC4 [23] (or referring to simple superposition method) yields accurate predictions for the elliptical CFST column, given as follows:

$$N_{u,EC4} = f_y A_s + f_c^{'} A_c \tag{8}$$

where f_y and $f_c^{'}$ are the yield strength of steel and cylinder compressive strength of concrete, respectively; A_s and A_c are the cross-sectional area of steel tube and concrete, respectively.

Zhao and Packer [3] and Jamaluddin et al. [7] found that the design method for circular CFST columns in EC4 considering the confinement effect can be used for elliptical CFST columns, if an equivalent diameter is used for the elliptical section.

$$N_{u,EC4} = \eta_s f_y A_s + \left[1 + \eta_c \left(\frac{t_s}{D_e}\right)\left(\frac{f_y}{f_c^{'}}\right)\right] f_c^{'} A_c \tag{9}$$

when evaluating the cross-sectional behaviour, the factor η_s=0.75 and η_c=4.9.

The equivalent diameter D_e can be calculated by equations proposed by Gardner and Chan [24] or Ruiz-Teran and Gardner [25], given as follows:

$$D_e = 2a \cdot (a/b) \tag{10}$$

or:

$$D_e = 2a \cdot \left[1 + f \cdot (a/b - 1)\right] \tag{11}$$

$$f = 1 - 2.3 \cdot (t_s / 2a)^{0.6} \tag{12}$$

Uenaka [4] advised to calculate the load-bearing capacity of the elliptical CFST columns with the following equation based on his test results:

$$N_{u,Uenaka} = 1.46\left(f_y A_s + f_c' A_c \right) \quad (13)$$

Most of above methods have been validated by test results of the elliptical CFST columns with an aspect ratio of 2.0, which is the only product type of the hot-rolled elliptical hollow section. For cold-formed elliptical sections, the aspect ratio can vary continuously, which means the confinement effect will be significant if the aspect ratio is close to 1.0. Therefore the above methods need to be further validated against test and FE results of elliptical CFST columns with different aspect ratios. The tests in this study, together with tests conducted by Yang et al. [2], Zhao and Packer [3], Uenaka [4], Chan et al. [5] and Jamaluddin et al. [7], and FE results in this study were employed to validate the above design methods. The comparisons are presented in Fig.16.

As observed, the method provided by GB50936-2014 can accurately predict the load-bearing capacity of elliptical CFST columns with aspect ratio ranging from 1.0 to 2.5. The simple superposition method yields reasonable predictions for specimens with an aspect ratio equal or larger than 2.0, however, the predictions would be over conservative while the aspect ratio is smaller than 2.0. The design method for circular CFST columns in EC4, which considers the confinement effect, can be successfully used for elliptical CFST columns by using equivalent diameter approach. For some circular CFST columns (a/b=1.0), this method gives unconservative predictions. Because there is no descending phase of the load versus displacement curves of these columns, the load corresponding to 3000 με was taken as the ultimate load [13] in the FE analysis. This may be different from the criteria of the method in EC4. The above comparisons confirm that it is reasonable to take the effect of aspect ratio into account in the design methods for predicting load-bearing capacities of elliptical CFST columns.

5. Conclusions

The behaviours of concrete-filled cold-formed elliptical hollow sections were studied experimentally and numerically in this study. Twenty one specimens were tested to investigate the fundamental behaviours of these elliptical CFST columns and to obtain data for FE model validation. A stress versus strain relationship model was proposed for concrete in elliptical CFST columns and a FE model was developed using program ABAQUS. Parametric studies were

performed to identify the influence of key parameters on the behaviours of these columns. And related design methods were evaluated for their applicability for elliptical CFST columns. Based on these studies, the following conclusions can be drawn:

(1) The axially loaded elliptical CFST stub columns all failed by shear failure, while ductile behaviour was observed due to the confinement effect. The transverse stress in the elliptical steel tube is not uniform along the perimeter, which gradually decreases from the maximum value at the end of minor axis to the minimum value at the end of major axis.

(2) Both the load-bearing capacity and the ductility decrease noticeably with the increasing aspect ratio, due to the deterioration of confinement effect. The increasing steel tube to concrete area ratio and yield strength of steel enhances the load-bearing capacity and ductility. The increase of concrete strength also increases the load-bearing capacity, but, the ductility of the corresponding column declines due to the more brittle behaviour of the higher strength concrete.

(3) The proposed stress versus strain relationship model for the concrete in elliptical CFST columns yields good predictions for elliptical CFST stub columns with different aspect ratios. Further studies will be needed to simulate elliptical CFST slender columns subjected to compression, bending and combined loading conditions.

(4) The design method for elliptical CFST columns in Chinese code GB50936-2014 and the method for circular CFST columns in EC4 can be successfully used for predicting the cross-sectional capacity of the elliptical CFST stub column with varying aspect ratio from 1.0 to 2.5. An equivalent diameter should be used in the latter method, which means the effect of aspect ratio is also taken into account. If the aspect ratio exceeds 2.0, the simple superposition method also generates good predictions.

6. Acknowledgement

The research presented in this paper was sponsored by the National Natural Science Foundation (No. 51378152), Excellent Young Talents Program of Harbin Institute of Technology and Hei Long Jiang Postdoctoral Foundation (LBH-Z15086); their financial support is highly appreciated.

7. References

[1] Chan TM, Gardner L, Law KH. Structural design of elliptical hollow sections: a review. Proceedings of the ICE-Structures and Buildings. 2010;163:391-402.

[2] Yang H, Lam D, Gardner L. Testing and analysis of concrete-filled elliptical hollow sections. Engineering Structures. 2008;30:3771-81.

[3] Zhao XL, Packer JA. Tests and design of concrete-filled elliptical hollow section stub columns. Thin-Walled Structures. 2009;47:617-28.

[4] Uenaka K. Experimental study on concrete filled elliptical/oval steel tubular stub columns under compression. Thin-Walled Structures. 2014;78:131-7.

[5] Chan TM, Huai YM, Wang W. Experimental investigation on lightweight concrete-filled cold-formed elliptical hollow section stub columns. Journal of Constructional Steel Research. 2015;115: 434-44.

[6] Sheehan T, Dai XH, Chan TM, Lam D. Structural response of concrete-filled elliptical steel hollow sections under eccentric compression. Engineering Structures. 2012;45:314-23.

[7] Jamaluddin N, Lam D, Dai XH, Ye J. An experimental study on elliptical concrete filled columns under axial compression. Journal of Constructional Steel Research. 2013;87:6-16.

[8] Dai X, Lam D. Numerical modelling of the axial compressive behaviour of short concrete-filled elliptical steel columns. Journal of Constructional Steel Research. 2010;66:931-42.

[9] Dai XH, Lam D, Jamaluddin N, Ye J. Numerical analysis of slender elliptical concrete filled columns under axial compression. Thin-Walled Structures. 2014;77:26-35.

[10] Espinos A, Romero ML, Portolés JM, Hospitaler A. Ambient and fire behavior of eccentrically loaded elliptical slender concrete-filled tubular columns. Journal of Constructional Steel Research. 2014;100:97-107.

[11] Ren QX, Han LH, Lam D, Li W. Tests on elliptical concrete filled steel tubular (CFST) beams and columns. Journal of Constructional Steel Research. 2014;99:149-60.

[12] McCann F, Gardner L, Qiu W. Experimental study of slender concrete-filled elliptical hollow section beam-columns. Journal of Constructional Steel Research. 2015;113:185-94.

[13] Zhong ST. The concrete-filled steel tubular structures. Tsinghua University Press. 2003 (in Chinese)

[14] GB/T 228-2010. Metallic materials-Tensile testing-Part 1: Method of test at room temperature. Beijing: China Standard Press. 2010 (in Chinese)

[15] Liu F, Gardner L, Yang H. Post-fire behaviour of reinforced concrete stub columns confined by circular steel tubes. Journal of Constructional Steel Research. 2014;102:82-103.

[16] Zhang S, Guo L, Ye Z, Wang Y. Behavior of steel tube and confined high strength concrete for concrete-filled RHS tubes. Advances in Structural Engineering. 2005;8:101-16.

[17] Han LH, Yao GH, Tao Z. Performance of concrete-filled thin-walled steel tubes under pure torsion. Thin-Walled Structures. 2007;45:24-36.

[18] Committee A, Institute AC, Standardization IOf. Building code requirements for structural concrete (ACI 318-08) and commentary. American Concrete Institute; 2008.

[19] Chan TM, Gardner L. Compressive resistance of hot-rolled elliptical hollow sections. Engineering Structures. 2008;30(2):522-32.

[20] Theofanous M, Chan TM, Gardner L. Structural response of stainless steel oval hollow section compression members. Engineering Structures. 2009;31(4):922-34.

[21] Tao Z, Wang ZB, Yu Q. Finite element modelling of concrete-filled steel stub columns under axial compression. Journal of Constructional Steel Research. 2013;89:121-31.

[22] GB50936-2014. Technical code for concrete filled steel tubular structures. Ministry of Housing and Urban-Rural Development of the People's Republic of China. 2014 (in Chinese)

[23] CEN CEdN. Eurocode 4: Design of composite steel and concrete structures-Part 1.1: General-General rules and rules for buildings. EN 1994-1-1, Brussels; 2004.

[24] Gardner L, Chan TM. Cross-section classification of elliptical hollow sections. Steel and Composite Structures. 2007;7:185-200.

[25] Ruiz-Teran AM, Gardner L. Elastic buckling of elliptical tubes. Thin-Walled Structures. 2008;46:1304-18.

Figures captions

Table captions

aTable 1 Detailed parameters of the specimens

Column No.	$2a$ (mm)		$2b$ (mm)		t_s (mm)		Designed H (mm)	a/b	Nominal α_s (%)
	Designed	Measured	Designed	Measured	Nominal	Measured			
CH20-a	203.3	200.0	101.6	100.5	2.75	2.60	407	2.0	–
CH20-b	203.3	201.0	101.6	101.5	2.75	2.60	407	2.0	–
CH20-c	203.3	201.2	101.6	101.7	2.75	2.61	407	2.0	–
C10-8-a	135.3	136.5	135.3	136.5	2.75	2.63	271	1.0	8.0
C10-8-b	135.3	137.0	135.3	137.0	2.75	2.61	271	1.0	8.0
C10-8-c	135.3	137.8	135.3	137.8	2.75	2.64	271	1.0	8.0
C15-8-a	169.2	170.0	112.8	112.0	2.75	2.62	338	1.5	8.0
C15-8-b	169.2	169.6	112.8	111.0	2.75	2.61	338	1.5	8.0
C15-8-c	169.2	168.0	112.8	112.5	2.75	2.60	338	1.5	8.0
C20-8-a	203.3	202.0	101.6	99.0	2.75	2.60	407	2.0	8.0
C20-8-b	203.3	199.8	101.6	100.8	2.75	2.60	407	2.0	8.0
C20-8-c	203.3	201.5	101.6	100.4	2.75	2.59	407	2.0	8.0
C25-8-a	237.5	236.0	95.0	95.8	2.75	2.62	475	2.5	8.0
C25-8-b	237.5	237.5	95.0	96.0	2.75	2.58	475	2.5	8.0
C25-8-c	237.5	236.0	95.0	96.5	2.75	2.61	475	2.5	8.0
C20-5-a	318.0	318.0	159.0	155.0	2.75	2.59	636	2.0	5.0
C20-5-b	318.0	318.5	159.0	151.5	2.75	2.60	636	2.0	5.0
C20-5-c	318.0	317.0	159.0	153.5	2.75	2.60	636	2.0	5.0
C20-12-a	139.6	139.0	69.8	68.0	2.75	2.59	279	2.0	12.0
C20-12-b	139.6	138.0	69.8	68.2	2.75	2.61	279	2.0	12.0
C20-12-c	139.6	137.5	69.8	68.0	2.75	2.58	279	2.0	12.0

Table 2 Properties of the steel tube

Nominal t_s (mm)	Measured t_s (mm)	E_s (N/mm^2)	f_y (N/mm^2)	f_u (N/mm^2)	ν_s	ε_f (%)
2.75	2.60	1.85×10^5	376.4	464.9	0.23	28.9

Table 3 Concrete mixtures and tested strengths

Water (kg/m^3)	Cement (kg/m^3)	Fines (kg/m^3)	Coarse (kg/m3)	Super-plasticiser (kg/m^3)	$f_{cu,28}$ (N/mm^2)	$f_{cu,test}$ (N/mm^2)	$E_{c,test}$ (N/mm^2)
215.0	545.4	524.7	1114.9	1.1	57.0	63.1	2.585×10^4

Table 4 Test results of the specimens

Column No.	N_y (kN)	Δ_y (mm)	N_u (kN)	Δ_u (mm)	$\Delta_{0.85}$ (mm)	μ_Δ	σ_{aver} (N/mm^2)
CH20-a	379.5	0.97	420.6	1.40	2.14	1.52	348.7
CH20-b	391.8	0.90	440.9	1.28	2.21	1.73	363.1
CH20-c	404.1	1.00	440.3	1.37	2.52	1.84	360.8
Average	*391.8*	*0.96*	*434.0*	*1.35*	*2.29*	*1.70*	*357.5*
C10-8-a	1122.9	1.03	1296.3	2.32	4.89	2.10	88.6
C10-8-b	1143.1	0.95	1325.3	2.16	5.89	2.73	89.9
C10-8-c	1169.0	0.97	1343.0	3.39	8.24	2.43	90.1
Average	*1145.0*	*0.98*	*1321.5*	*2.62*	*6.34*	*2.42*	*89.5*
C15-8-a	1109.2	0.79	1310.6	1.74	3.86	2.22	87.6
C15-8-b	1146.1	1.23	1299.2	2.44	5.11	2.09	87.9
C15-8-c	1127.9	1.10	1294.4	2.37	4.68	1.97	87.2
Average	*1127.7*	*1.04*	*1301.4*	*2.19*	*4.55*	*2.09*	*87.6*
C20-8-a	1135.3	0.95	1298.7	1.64	2.28	1.39	82.7
C20-8-b	1162.4	1.01	1325.0	1.85	2.49	1.35	83.8
C20-8-c	1239.9	1.00	1381.1	1.69	3.04	1.80	86.9
Average	*1179.2*	*0.99*	*1334.9*	*1.73*	*2.60*	*1.51*	*84.5*
C25-8-a	1195.0	1.00	1309.2	1.78	2.15	1.21	73.7
C25-8-b	1197.3	1.11	1364.6	1.81	2.29	1.27	76.2
C25-8-c	1215.5	1.15	1354.2	1.95	2.62	1.34	75.7
Average	*1202.6*	*1.09*	*1342.7*	*1.85*	*2.36*	*1.27*	*75.2*
C20-5-a	2404.0	1.10	2607.0	1.50	2.32	1.54	67.3
C20-5-b	2408.4	1.24	2497.3	1.42	3.12	2.20	65.9
C20-5-c	2298.5	1.42	2521.5	1.92	2.88	1.50	66.0
Average	*2370.3*	*1.25*	*2542.0*	*1.61*	*2.77*	*1.75*	*66.4*
C20-12-a	610.4	0.70	687.2	1.45	3.64	2.51	92.6
C20-12-b	624.1	0.82	688.1	1.43	3.49	2.44	93.1
C20-12-c	620.1	0.68	699.2	1.24	2.22	1.80	95.2
Average	*618.2*	*0.73*	*691.5*	*1.37*	*3.12*	*2.25*	*93.6*

Table 5 Comparisons between FE and test results in this study

Column No.	$N_{u,test}$ (kN)	$N_{u,FE}$ (kN)	$\Delta_{u,test}$ (mm)	$\Delta_{u,FE}$ (mm)	$N_{u,FE}/N_{u,test}$	$\Delta_{u,FE}/\Delta_{u,test}$
C10-8-a	1296.3	1364	2.33	1.98	1.05	0.85
C10-8-b	1325.3	1364	2.25	1.98	1.03	0.88
C10-8-c	1343	1364	2.70	1.98	1.02	0.74
C15-8-a	1310.6	1262	1.82	1.48	0.96	0.81
C15-8-b	1299.2	1262	2.43	1.48	0.97	0.61
C15-8-c	1294.4	1262	2.38	1.48	0.97	0.62
C20-8-a	1298.7	1314	1.65	1.38	1.01	0.84
C20-8-b	1325	1314	1.70	1.38	0.99	0.82
C20-8-c	1381.1	1314	1.53	1.38	0.95	0.91
C25-8-a	1309.2	1472	1.78	1.38	1.12	0.78
C25-8-b	1364.6	1472	1.40	1.38	1.08	0.99
C25-8-c	1354.2	1472	1.95	1.38	1.09	0.71
C20-5-a	2607	2685	1.50	1.88	1.03	1.26
C20-5-b	2497.3	2685	1.40	1.88	1.08	1.35
C20-5-c	2521.5	2685	1.82	1.88	1.06	1.04
C20-12-a	687.2	706	1.37	1.08	1.03	0.79
C20-12-b	688.1	706	1.23	1.08	1.03	0.88
C20-12-c	699.2	706	1.53	1.08	1.01	0.71
Average					*1.027*	*0.866*

Table 6 Comparisons between FE and test ultimate loads

Column No.	$2a$ (mm)	$2b$ (mm)	t_s (mm)	H (mm)	a/b	f_y (MPa)	f_c' (MPa)	$N_{u,test}$ (kN)	$N_{u,FE}$ (kN)	$N_{u,FE}/N_{u,test}$	Sources
150×75×4-C30	150.4	75.6	4.18	300	2.0	376.5	30.5	839	829	0.99	Yang et al.[2]
150×75×4-C60	150.57	75.52	4.19	300	2.0	376.5	55.3	974	1011	1.04	
150×75×4-C100	150.39	75.67	4.18	300	2.0	376.5	102.2	1265	1371	1.08	
150×75×5-C30	150.12	75.65	5.12	300	2.0	369	30.5	981	914	0.93	
150×75×5-C60	150.23	75.74	5.08	300	2.0	369	55.3	1084	1085	1.00	
150×75×5-C100	150.28	75.67	5.09	300	2.0	369	102.2	1296	1438	1.11	
150×75×6.3-C30	148.78	75.45	6.32	300	2.0	400.5	30.5	1193	1089	0.91	
150×75×6.3-C60	148.92	75.56	6.43	300	2.0	400.5	55.3	1280	1294	1.01	
150×75×6.3-C100	149.53	75.35	6.25	300	2.0	400.5	102.2	1483	1625	1.10	
EHS1-SCC-Full	150.18	75.21	4.51	500	2.0	395	69.2	1075	1205	1.12	Zhao and Packer [3]
EHS2-SCC-Full	150.49	75.26	5.41	500	2.0	358	69.2	1163	1253	1.08	
EHS3-SCC-Full	150.05	75.42	6.56	500	2.0	369	69.2	1310	1377	1.05	
EHS4-SCC-Full	200.21	100.12	5.2	600	2.0	397	69.2	1598	1982	1.24	
EHS5-SCC-Full	200	100.35	6.1	600	2.0	411	69.2	2068	2236	1.08	
EHS6-SCC-Full	200.6	100.02	8.17	600	2.0	383	69.2	2133	2395	1.12	
EHS7-SCC-Full	200.19	100.41	9.72	600	2.0	367	69.2	2290	2512	1.10	
EHS8-NC-Full	220.7	110.7	6.16	698	2.0	421	48.2	2109	2398	1.14	

Table 6 Comparisons between FE and test ultimate load (continue)

Column No.	$2a$ (mm)	$2b$ (mm)	t_s (mm)	H (mm)	a/b	f_y (MPa)	f_c' (MPa)	$N_{u,test}$ (kN)	$N_{u,FE}$ (kN)	$N_{u,FE}/N_{u,test}$	Sources
e10-15-160	160	107.8	1	160	1.5	207	27.3	768.7	518.022	0.67	
e16-15-160	159.4	106.5	1.6	160	1.5	296	27.3	844	650.37	0.77	
e23-15-160	159.7	107.4	2.3	160	1.5	341	27.3	921.3	841.699	0.91	
e10-15-250	159.9	105.5	1	250	1.5	207	27.3	681.3	469.96	0.69	
e16-15-250	160.1	105.5	1.6	250	1.5	296	27.3	783.3	607.612	0.78	
e23-15-250	160.8	107	2.3	250	1.5	341	27.3	850.7	787.357	0.93	
e10-20-160	160.4	77.3	1	160	2.0	211	25	389.1	325.655	0.84	
e16-20-160	159.4	80.5	1.6	160	2.0	279	25	699.7	434.621	0.62	
e23-20-160	158.8	80.7	2.3	160	2.0	201	25	761.5	431.777	0.57	
e10-20-250	160.8	74.9	1	250	2.0	211	25	468.4	303.095	0.65	
e16-20-250	159.3	79.8	1.6	250	2.0	279	25	666.4	459.816	0.69	Uenaka [4]
e23-20-250	158.3	82	2.3	250	2.0	201	25	630.1	423.392	0.67	
e10-25-160	159.2	63.2	1	160	2.5	207	27.3	496	285.804	0.58	
e16-25-160	159.6	63.1	1.6	160	2.5	296	27.3	500.6	394.728	0.79	
e23-25-160	159.5	64.2	2.3	160	2.5	341	27.3	665.3	513.271	0.77	
e10-25-250	158.5	64.5	1	250	2.5	207	27.3	413.3	287.582	0.70	
e16-25-250	159.3	63.1	1.6	250	2.5	296	27.3	499.3	379.898	0.76	
e23-25-250	158.8	63.2	2.3	250	2.5	341	27.3	620.6	487.385	0.79	
e10-20-200	158.6	79.7	1	200	2.0	207	27.3	484.6	355.91	0.73	
e16-20-200	158	80.6	1.6	200	2.0	296	27.3	613.3	463.809	0.76	
e23-20-200	159.2	82.1	2.3	200	2.0	341	27.3	724	612.996	0.85	

Table 6 Comparisons between FE and test ultimate load (continue)

Column No.	$2a$ (mm)	$2b$ (mm)	t_s (mm)	H (mm)	a/b	f_y (MPa)	f_c' (MPa)	$N_{u,test}$ (kN)	$N_{u,FE}$ (kN)	$N_{u,FE}/N_{u,test}$	Sources
EF-A-SC1	119.6	59.8	5.4	250	2.0	599	31.2	864	1002.5	1.16	Chan et al.[5]
EF-A-SC2	119.5	60.1	5.4	250	2.0	599	31.2	857	1002.5	1.17	
EF-A-SC3	119.5	60.8	5.4	250	2.0	599	31.2	843	1002.5	1.19	
EF-C-SC1	119.9	57.9	8.7	250	2.0	578	31.2	1445	1342.7	0.93	
EF-C-SC2	119.8	58	8.9	250	2.0	578	31.2	1450	1342.7	0.93	
EF-C-SC3	119.9	57.9	8.8	250	2.0	578	31.2	1448	1342.7	0.93	
C1-150-C30	150.1	75	4.1	300	2.0	431.4	37.4	900	1032	1.15	Jamaluddin et al. [7]
C1-150-C60	150.2	75.1	4	301	2.0	431.4	36.2	1139	1004	0.88	
C1-150-C100	150.1	75.2	4.2	299	2.0	431.4	90	1239	1315	1.06	
C1-200-C30	197.8	100.1	5.1	398	2.0	431.4	35.2	1232	1519	1.23	
C1-200-C60	197.5	100.2	5.1	398	2.0	431.4	41.6	1737	1603	0.92	
C1-200-C100	197.4	100.1	5.1	398	2.0	431.4	72.3	2116	1900	0.90	

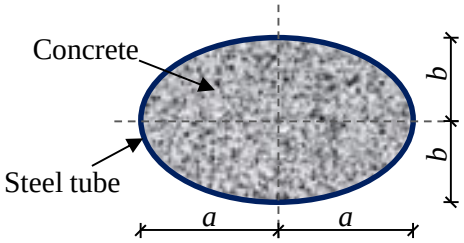

Fig.1 A schematic cross-section of an elliptical CSFT column.

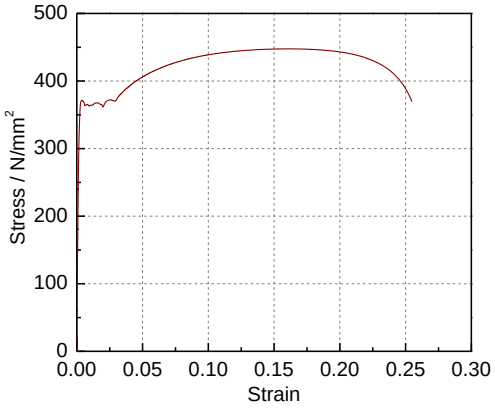

Fig.2 Measured stress versus strain relationship of the parent steel.

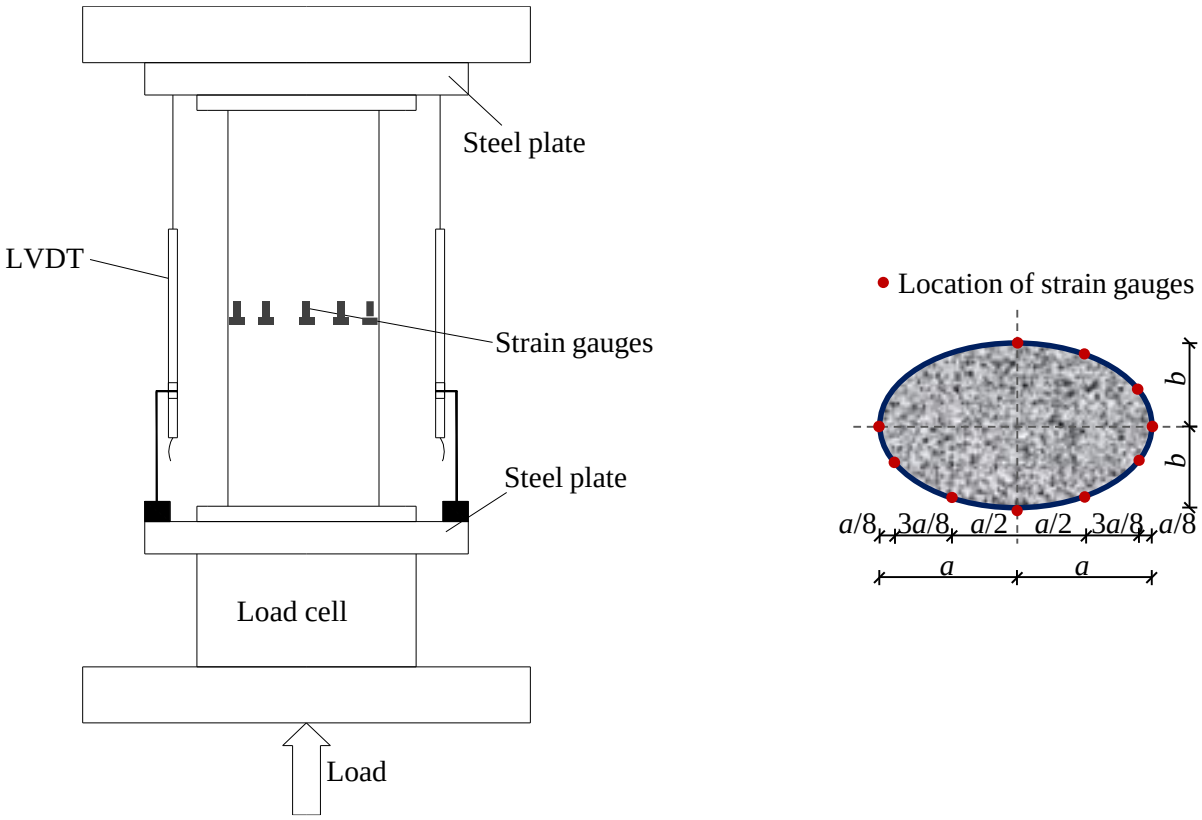

(a) (b)

Fig.3 Arrangement of instrumentations (a) transducers/strain gauges and (b) strain gauges.

(a) (b) (c)

(d) (e) (f)

(g)

Fig.4 Typical failure modes of specimens: (a) CH20; (b) C10-8; (c) C15-8; (d) C20-8; (e) C25-8; (f) C20-5; and (g) C20-12.

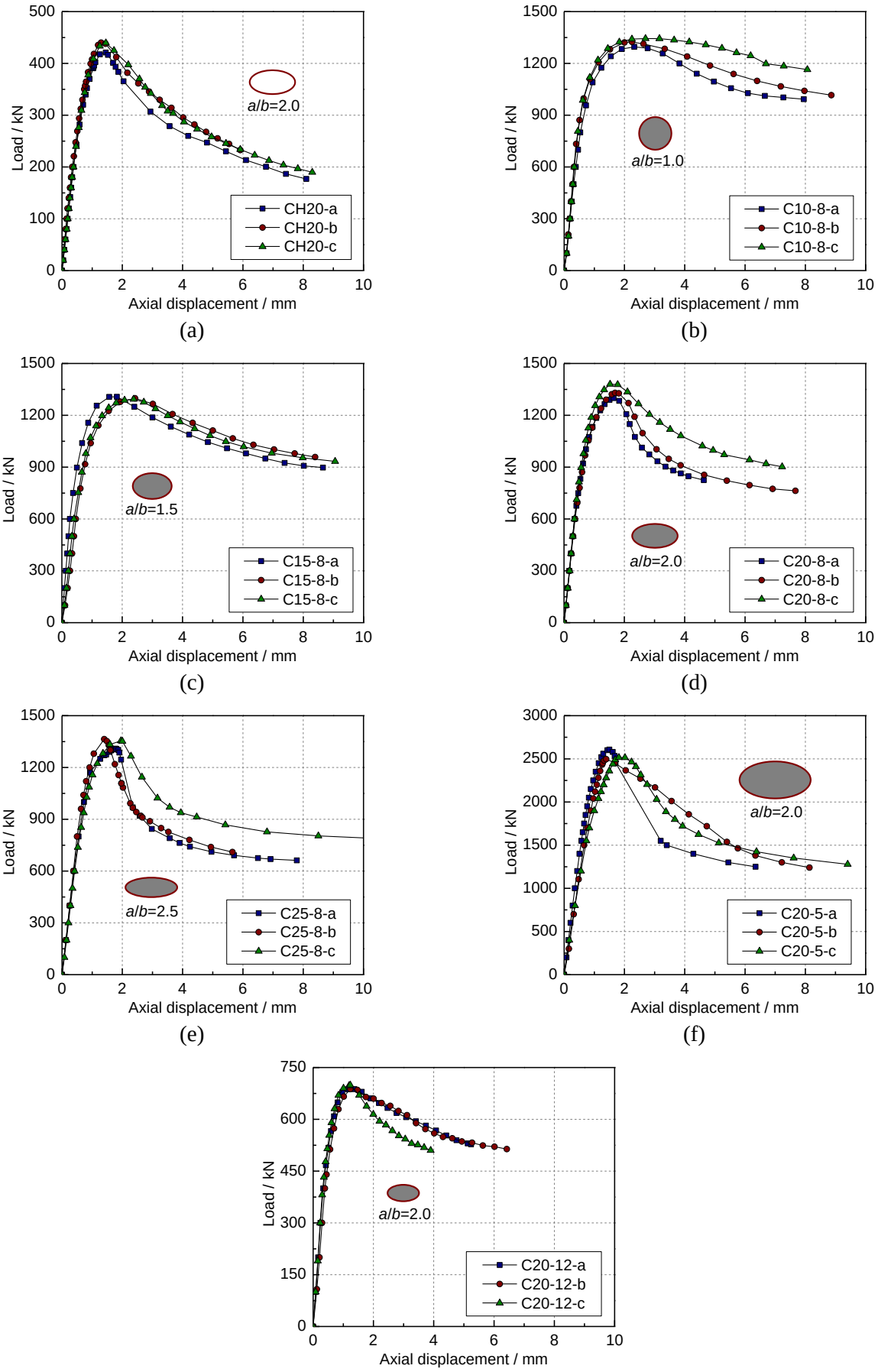

Fig.5 Load versus axial displacement curves of test specimens: (a) CH20; (b) C10-8; (c) C15-8; (d) C20-8; (e) C25-8; (f) C20-5; and (g) C20-12.

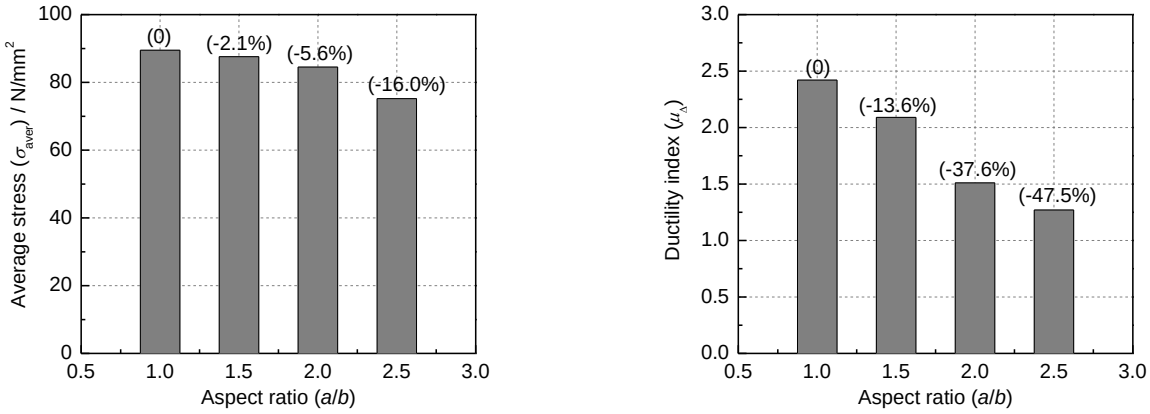

(a) (b)

Fig.6 Influence of aspect ratio on the: (a) average stress; and (b) ductility index.

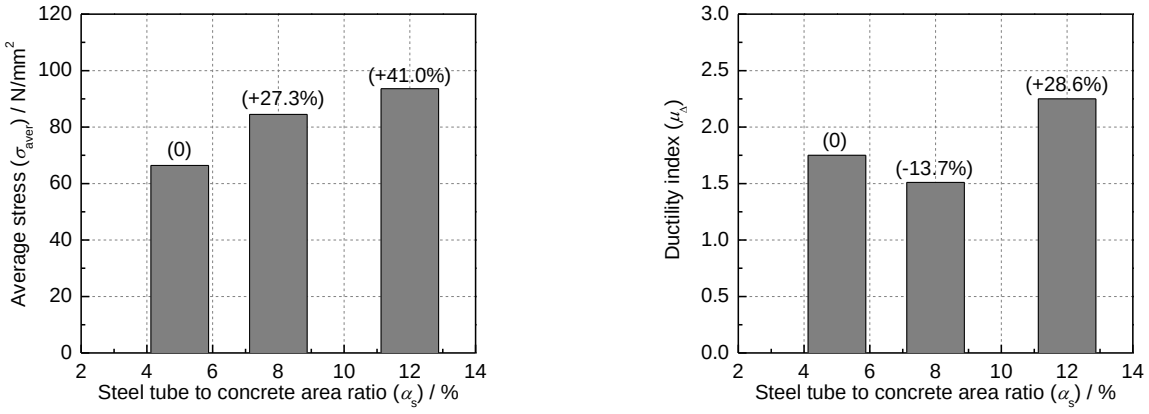

(a) (b)

Fig.7 Influence of steel tube to concrete area ratio on the: (a) average stress; and (b) ductility index.

(a) (b)

Fig.8 Typical locations of strain gauges across the section: (a) a/b=1.0; and (b) a/b=1.5, 2.0 and 2.5.

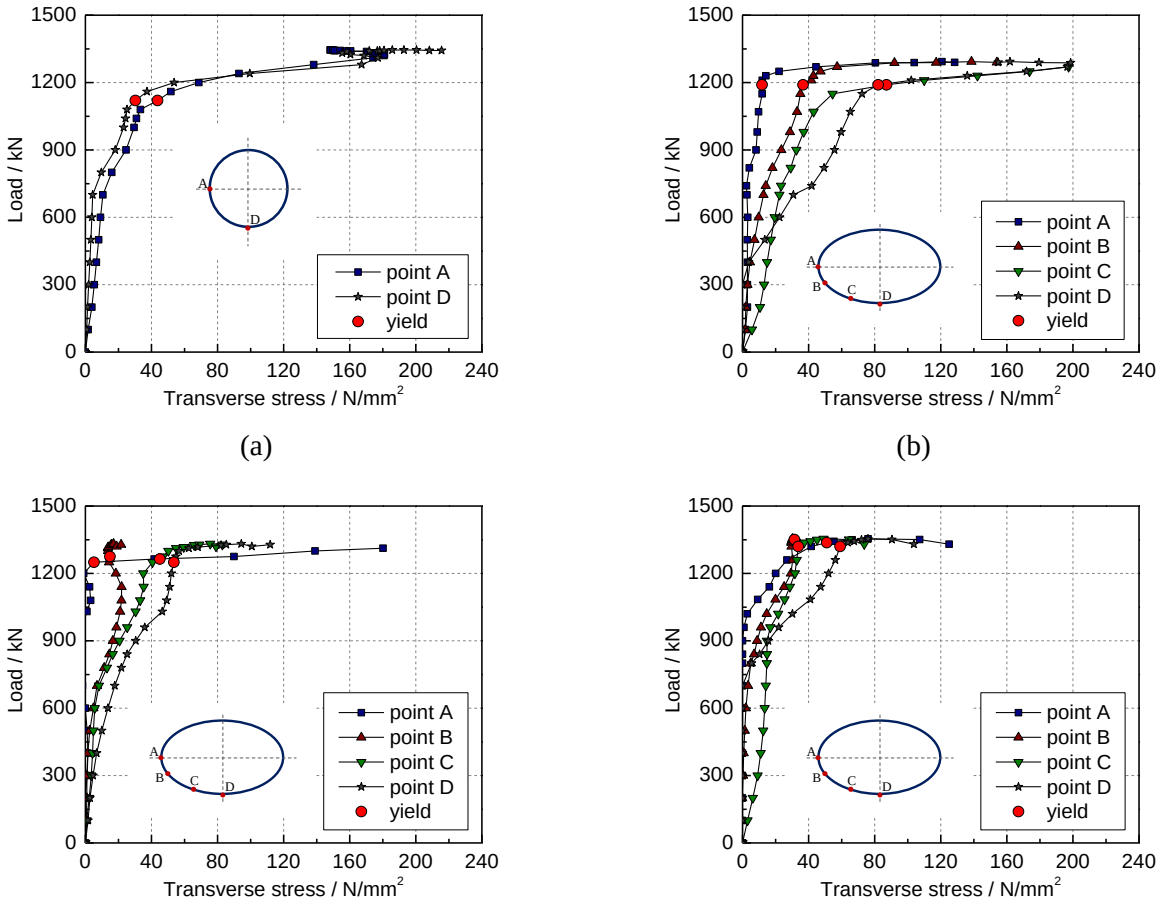

Fig.9 Transverse stresses in the steel tube of the elliptical CFST columns: (a) *a*/*b*=1.0 (C10-8); (b) *a*/*b*=1.5 (C15-8); (c) *a*/*b*=2.0 (C20-8); and (d) *a*/*b*=2.5 (C25-8).

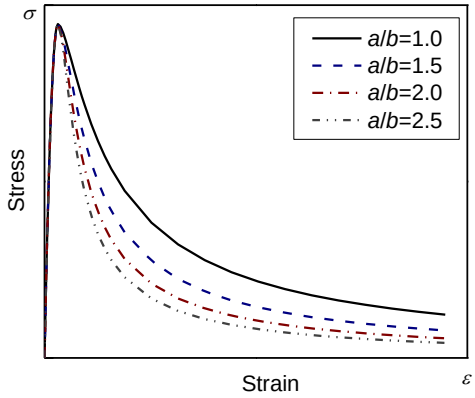

Fig.10 Proposed stress versus strain relationship of concrete.

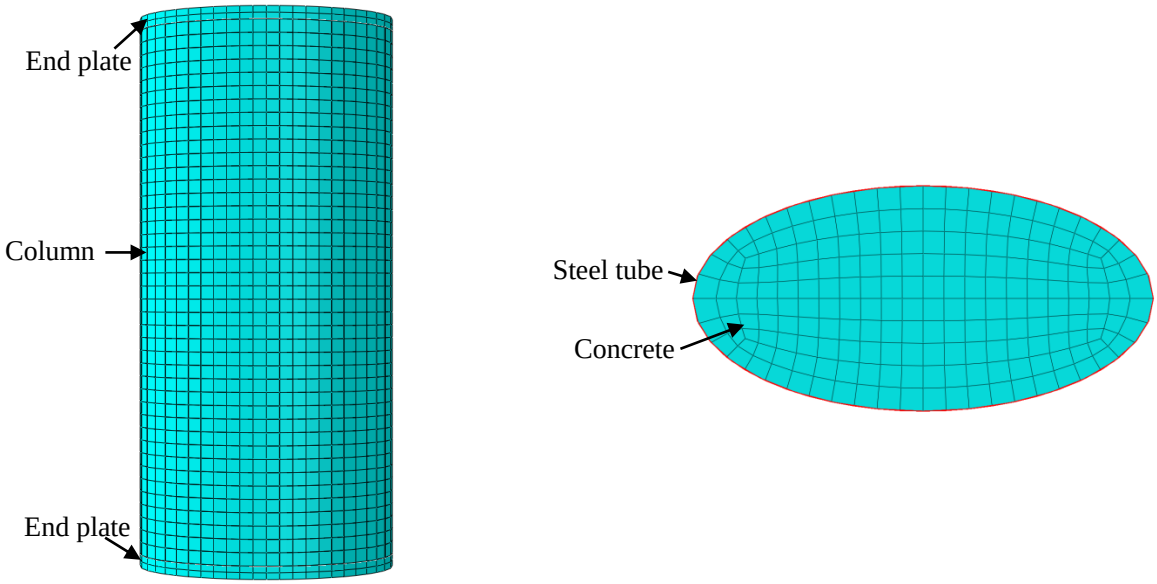

(a) (b)

Fig.11 FE model of the elliptical CFST column: (a) elevation; and (b) cross-section.

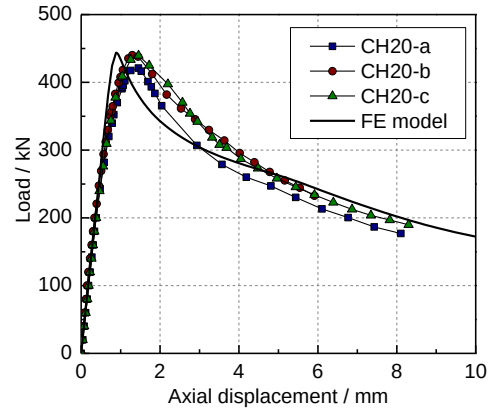

(a)

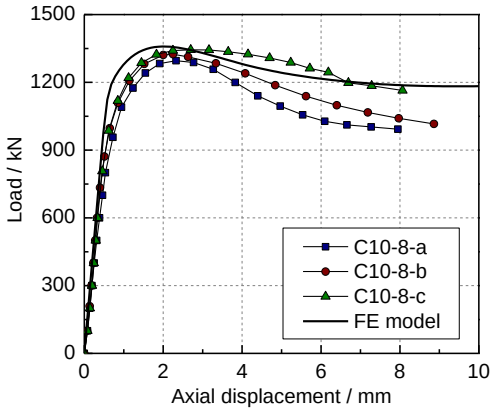

(b)

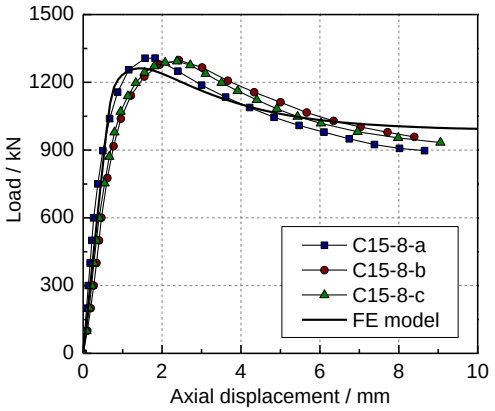

(c)

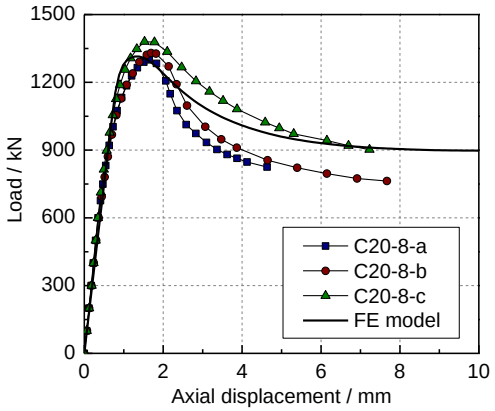

(d)

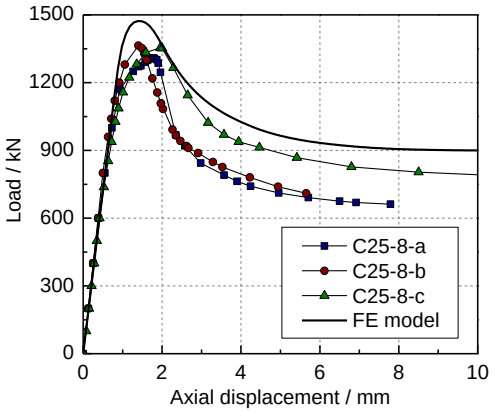

(e)

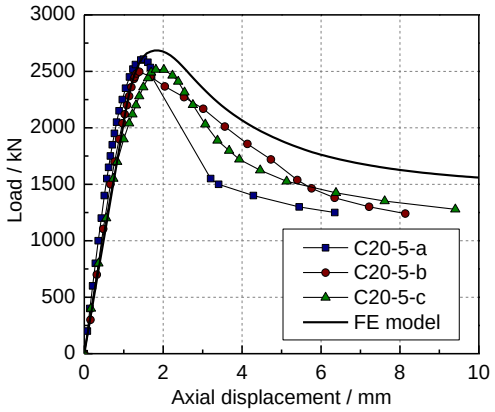

(f)

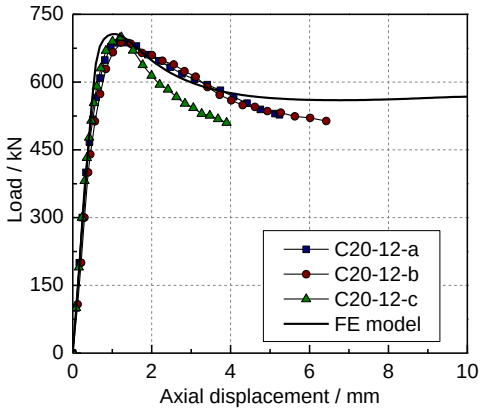

(g)

Fig.12 Comparisons between FE and test load versus axial displacement curves: (a) CH20; (b) C10-8; (c) C15-8; (d) C20-8; (e) C25-8; (f) C20-5; and (g) C20-12.

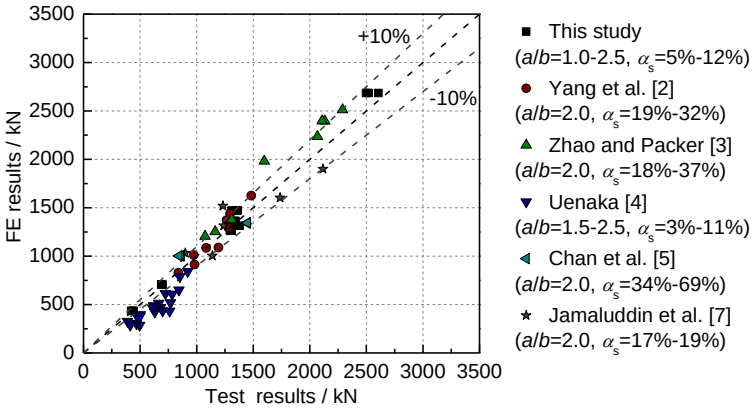

Fig.13 Comparisons between FE and test load-bearing capacities.

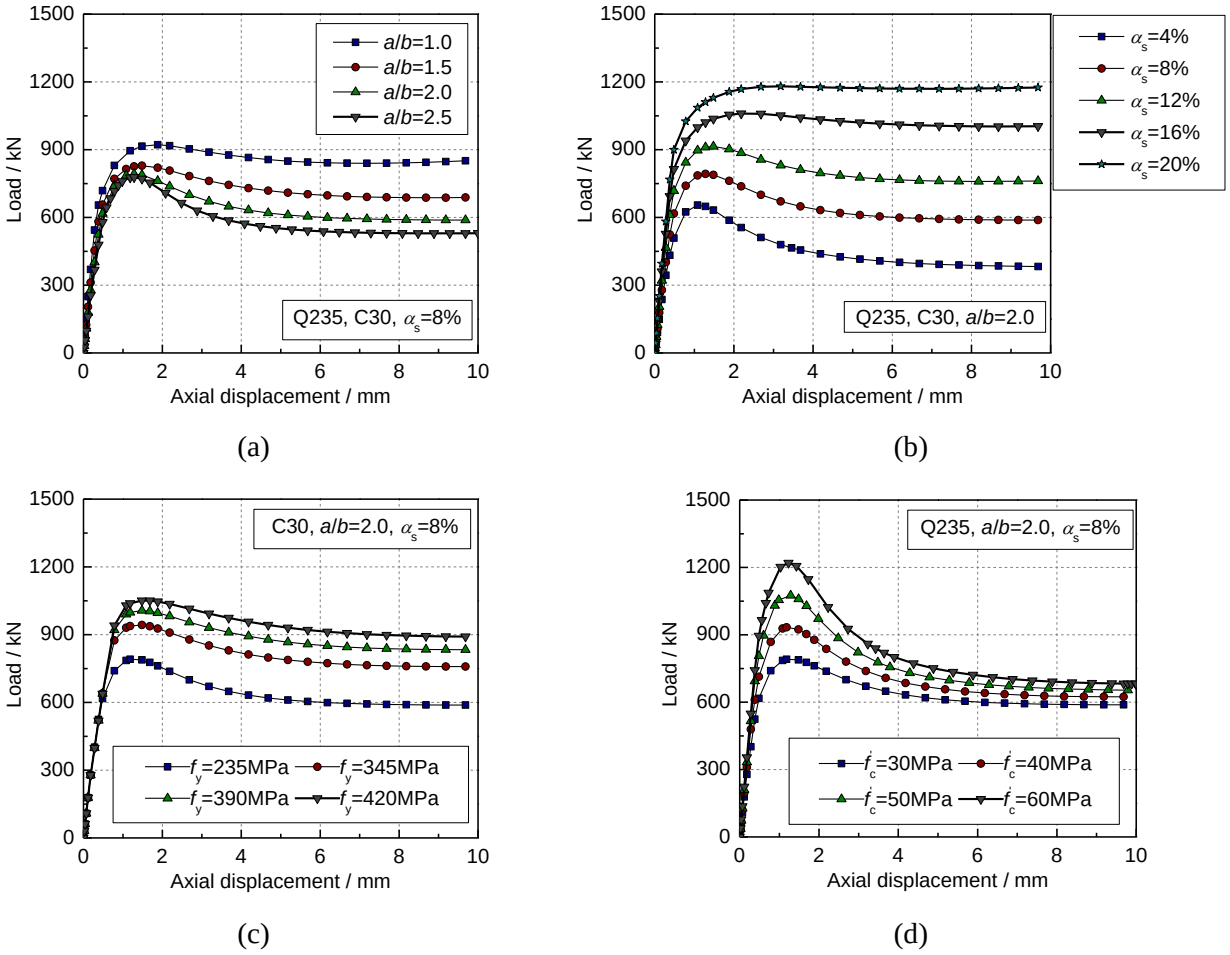

Fig.14 Influence of key parameters on the load versus axial displacement curves: (a) aspect ratio; (b) steel tube to concrete area ratio; (c) yield strength of steel; and (d) compressive strength of concrete.

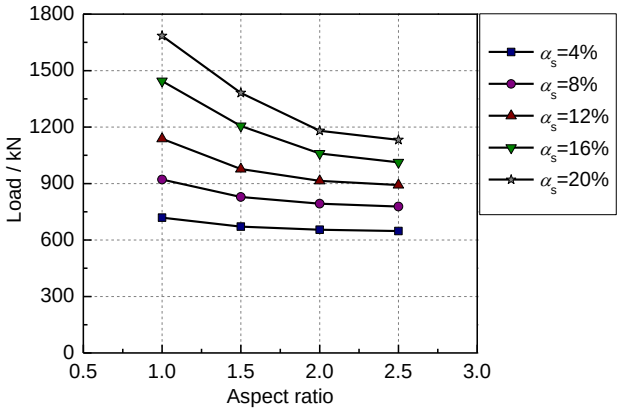

(a)

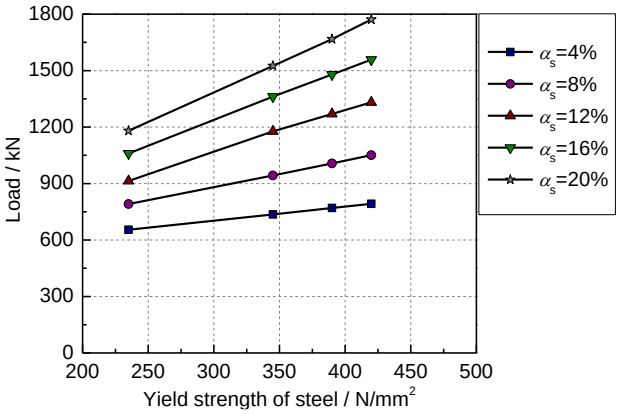

(b)

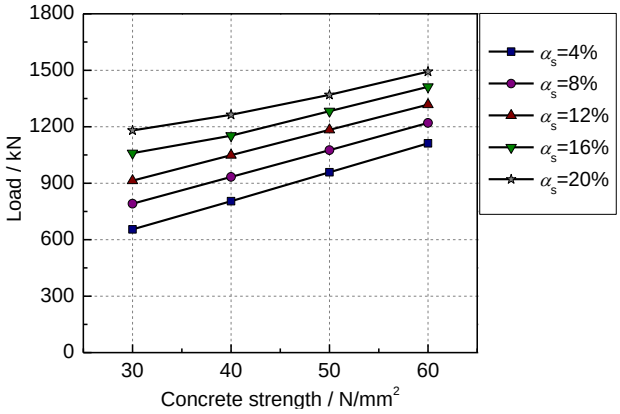

(c)

(d)

Fig.15 Influence of key parameters on the load-bearing capacity: (a) aspect ratio; (b) yield strength of steel; and (c) compressive strength of concrete.

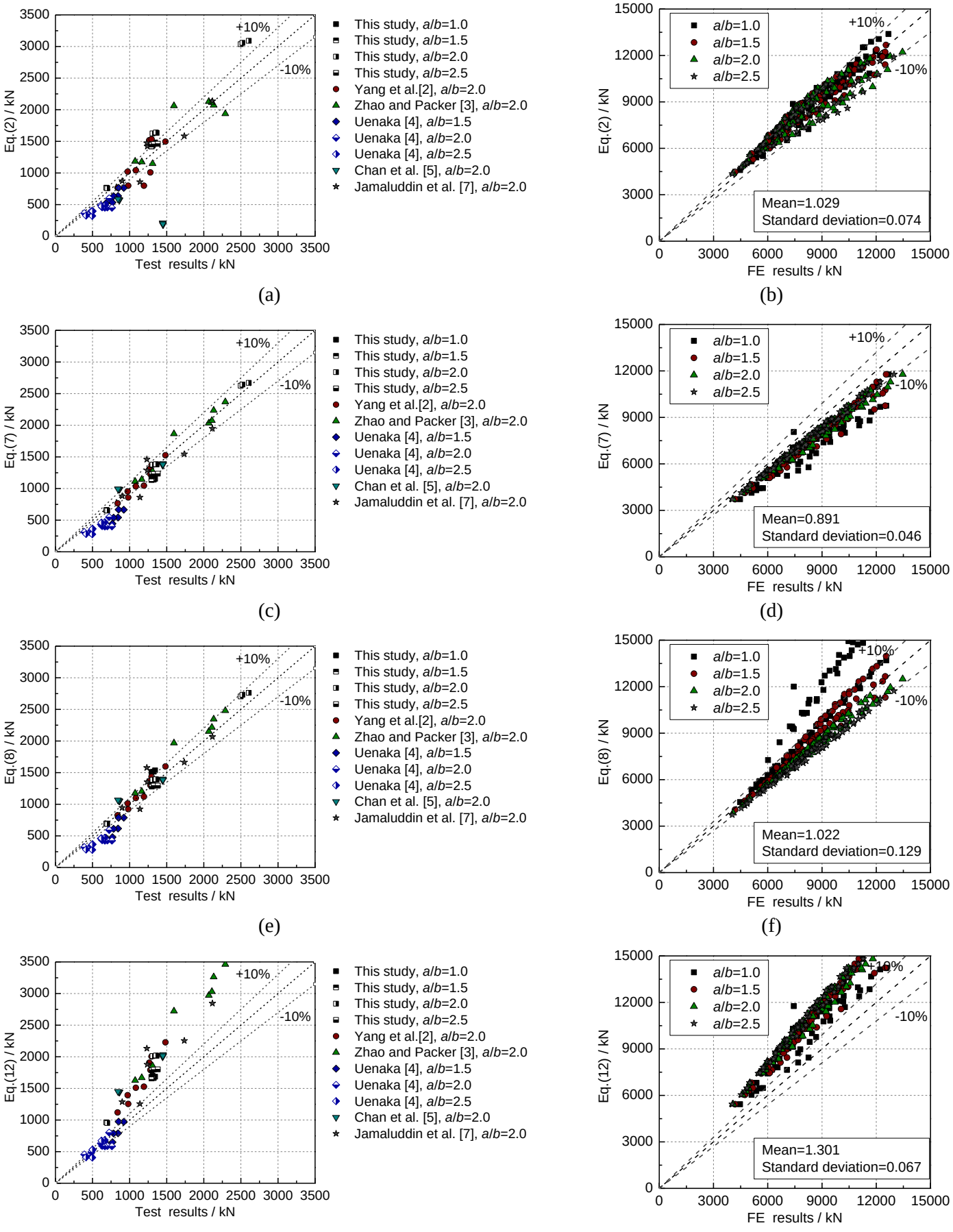

Fig.16 Comparisons between predictions of design method and test and FE results: (a) and (b): GB50936-2014; (c) and (d): simple superposition; (e) and (f): EC4; and (g) and (h): Uenaka.